UCRL-JC-128290 Rev 1
PREPRINT

The Fabrication and Testing of Optics for EUV Projection Lithography

J. S. Taylor
G. E. Sommargren
D. W. Sweeney
R. M. Hudyma

This paper was prepared for and presented at the
23rd Annual International Symposium on Microlithography
Santa Clara, California
February 22-27, 1998

March 18, 1998

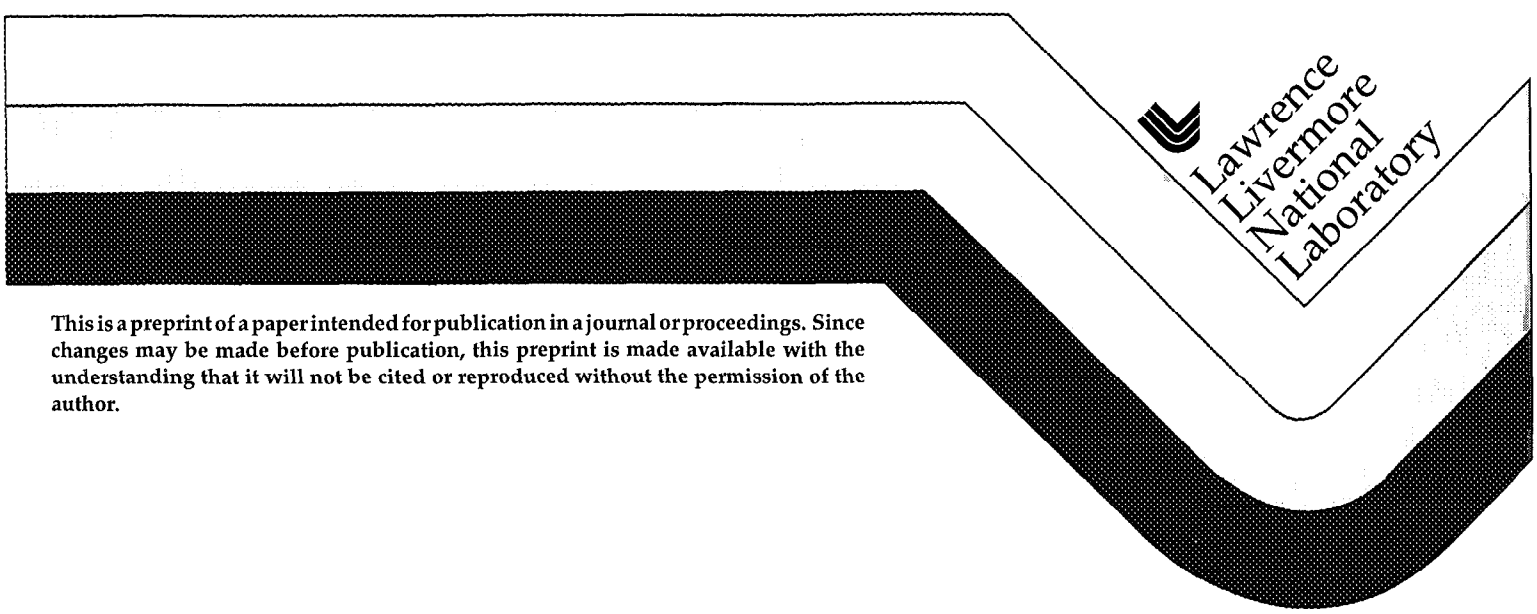

The Fabrication and Testing of Optics for EUV Projection Lithography

John S. Taylor, Gary E. Sommargren, Donald W. Sweeney, Russell M. Hudyma
Lawrence Livermore National Laboratory

Abstract

EUV Lithography (EUVL) is a leading candidate as a stepper technology for fabricating the "0.1 μm generation" of microelectronic circuits. EUVL is an optical printing technique qualitatively similar to DUV Lithography (DUVL), except that 11-13nm wavelength light is used instead of 193-248nm.[1,2] The feasibility of creating 0.1μm features has been well-established using small-field EUVL printing tools,[3] and development efforts are currently underway to demonstrate that cost-effective production equipment can be engineered to perform full-width ring-field imaging consistent with high wafer throughput rates.[4] Ensuring that an industrial supplier base will be available for key components and subsystems is crucial to the success of EUVL. In particular, the projection optics are the heart of the EUVL imaging system, yet they have figure and finish specifications that are beyond the state-of-the-art in optics manufacturing. Thus it is important to demonstrate that industry will be able to fabricate and certify these optics commensurate with EUVL requirements.

Indeed, the goal of this paper is to demonstrate that procuring EUVL projection optical substrates is feasible. This conclusion is based on measurements of both commercially-available and developmental substrates. The paper discusses EUVL figure and finish specifications, followed by examples of ultrasmooth and accurate surfaces, and concludes with a discussion of how substrates are measured and evaluated.

Specifications

EUVL projection systems employ all-reflective configurations in a ring field geometry with the mirror surfaces having stringent specifications on both figure and finish. Nominal specifications for the average allowable figure and finish errors on individual substrates for a 4-mirror EUVL projection optics design[4] are given in Table 1. These multi-mirror systems typically utilize aspheric surfaces to obtain aberration reduction, which adds a significant degree of difficulty to the fabrication and testing of the substrates.

Table 1. Nominal specifications for EUVL projection optics (4 mirror system).

Error Term	Maximum Error Specification	Defined by integrating the Power Spectral Density (PSD) of surface errors over the following bandlimits:
Figure	0.25 nm rms	(Clear Aperture)$^{-1}$ – 1 mm^{-1}
Mid-Spatial Frequency Roughness (MSFR)	0.20 nm rms	1 mm^{-1} – 1 μm^{-1}
High-Spatial Frequency Roughness (HSFR)	0.10 nm rms	1 μm^{-1} – 50 μm^{-1}

Wavefront error (WFE) requirements for diffraction-limited imaging scale with wavelength, and thus the evolution from DUV (λ = 193 nm) to EUV (λ = 13.4 nm) implies a factor of about 14x smaller allowable WFE for EUV systems.[5] If the projection optics are to achieve diffraction limited performance by Marechal's criterion, the composite wavefront error (at the exit pupil) must be less than $\lambda/14$ rms where λ is the operating wavelength.

This implies that the wavefront should have less than 1 nm rms deviation from a perfect sphere. In the context of our 4-mirror system, each surface should contribute, on the average, no more than 0.5 nm rms of WFE (assuming the errors are uncorrelated). For mirrors, the allowable surface figure error is one-half of the wavefront error; therefore the allowable average figure error for the 4-mirror system is 0.25 nm rms, which is the figure accuracy specified in Table 1.

Mid-spatial frequency roughness (MSFR) (spatial periods of 1 mm to 1 μm) causes near-angle scattering where the scattered light remains in the image field. Thus, MSFR causes a background illumination, usually referred to as *flare*, that is superimposed on the desired image. The most prominent effect of flare[6,7] is to reduce image contrast, which adversely limits the range of acceptable operating conditions (process window) for performing lithography. In addition, if the flare is non-uniform over the image field, then the critical dimensions (CD) of printed features will also exhibit non-uniformity.[8] Modeling efforts indicate that acceptable levels of image contrast and CD variation can be achieved for MSFR levels of 0.2 nm rms, as specified in Table 1. In the sense that near-angle scattering decreases the amount of energy that contributes to the useful image, it results in a decrease in reflectivity as would be measured with a reflectometer with a very small detector size. The relationship between flare and throughput is not simply stated, as it will depend on the bright-field/dark-field distribution in the image, and consideration of the amount of energy scattered back into the useful light regions of the image.

Wide-angle scattering is caused by high-spatial frequency roughness (HSFR) (spatial periods <1 μm) and results in a loss to the system because light is scattered outside of the image field. Wide-angle scattering also decreases contrast by reducing the intensity of the "light" areas of the image field, in comparison with near-angle scattering, which decreases contrast by redistributing energy within the image field.

The key that enables the use of normal-incidence optics in EUV imaging systems is multilayer coating technology,[9] which can provide reflectivities of 65-70%. Although reflectivity is dependent upon the properties of the multilayers, surface roughness is a major influence on reflectivity because it causes energy to be scattered outside of the image. The reflectivity from superpolished substrates with Mo/Si multilayers is about 67%, where the difference from the theoretical value of 74% is due to non-idealities of the multilayers, such as interlayer diffusion. For the high quality multilayers currently used, a decrease in reflectivity below 67% is correlated with scattering caused by substrate surface roughness.[10]

The fraction of energy that passes through a multi-mirror imaging system can be estimated by compounding the reflectivity (or losses) from each sequential bounce through the system. For a 4-mirror system where the mirrors have the same reflectivity, the throughput is simply the reflectivity raised to the fourth power. Figure 1 shows how dramatically imaging system throughput decreases as reflectivity drops for a 4-mirror system.[11] For our targeted reflectivity of 67%, the throughput is about 20%. Reflectivities below 67% are due to both near- and wide-angle scattering.

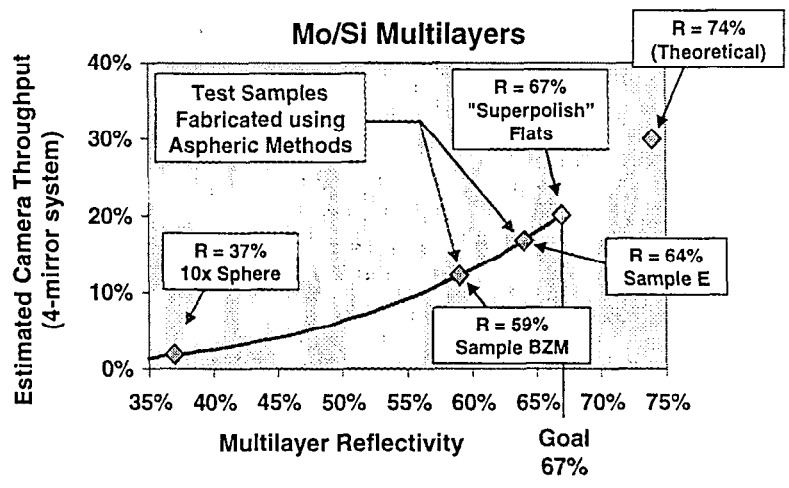

Figure 1. The dependence of system throughput on reflectivity for a four mirror system calculated as (reflectivity)^n; data points are for Mo/Si multilayers; Sample E reflectivity estimated from PSD.

The reflectivity of coated aspheric mirrors has lagged significantly behind the reflectivity from coated superpolished substrates. This difference is due to the increased level of roughness that has historically been observed on aspheric surfaces as a result of the fabrication methodologies required for aspheres. In Figure 1, the different data points indicate the evolution in surface quality that is leading to higher reflectivity. The sample labeled "10x Sphere" is indicative of the level of reflectivity obtained on both spherical and aspherical optical optics that are conventionally polished, i.e. not superpolished. A 4-mirror system with this 37% reflectivity would yield a dismal 2% in system throughput. Samples "BZM" and "E" are flat Zerodur M mirrors that were fabricated using aspherical techniques that have been recently developed by a commercial supplier. [The goals of these developmental samples will be discussed in a later section.] As indicated in the figure, these developmental substrates show much higher levels of reflectivity, which results in a substantially higher system throughput. As will be illustrated in the following sections, the HSFR data obtained from Sample E (aspheric processing) approaches the value obtained on superpolished surfaces. An important conclusion is that it is quite feasible that commercially-available aspheric EUVL substrates will attain the same reflectivity values as superpolished flats, i.e. 67% for Mo/Si, with the correspondingly higher level of system throughput.

The Evolution of Optical Fabrication to Meet EUVL Specifications

Figure 2 is a plot of surface errors for the three key specification categories (figure, MSFR, HSFR) versus the year in which they should be achieved in order to meet current program requirements; each of the three lines corresponds to a different category. The three points at 1997 ("Sandia 5x") are the measured values from aspheric surfaces fabricated for another project[12,13] and represent the state-of-the-art for combined figure and finish at the beginning of the current program. The fact that the MSFR is greater than the figure error is indicative of the impressive level of determinism in the figuring process, while also indicating that finish is often sacrificed during aspheric processing. In comparison, the data point labeled "CRADA" for mid-1996 represents an impressive 0.3 nm rms measured figure error, although finish was not specifically controlled for that optic.[14] The points indicated for 1998 and 1999 are the specifications for optics required in the current effort; the "intermediate specifications" in 1998 offer an interim milestone mid-way during the finishing process development that links the state-of-the-art in 1997 with the final requirements for 1999.

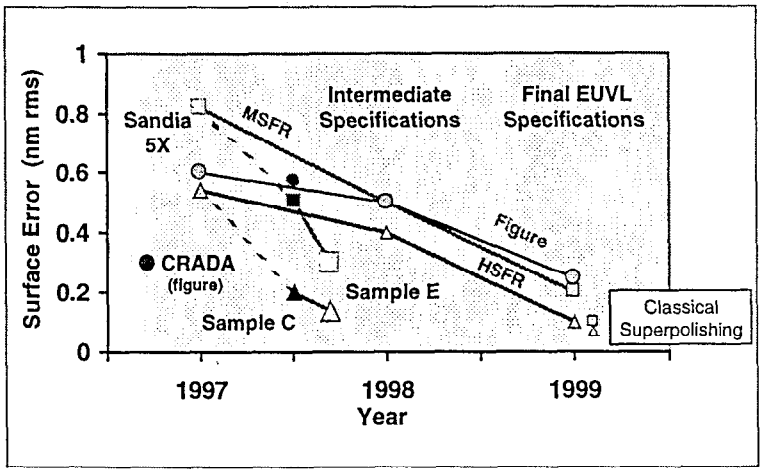

Figure 2. This timeline depicts how figure and finish specifications for EUVL are evolving to support current program requirements. Data points (Samples C and E) indicate that developments in aspheric manufacturing are rapidly approaching EUVL program goals.

The two points to the right of 1999 labeled as "Classical Superpolishing" are the levels of MSFR and HSFR that can be produced on flats and spheres by companies that perform "superpolishing", such as for laser gyro components.[15] These points represent a "proof of existence" that demonstrates that optical fabrication methods can indeed attain these levels of finish. For example, AFM micrographs of small lenses that are produced in production quantities are shown in Figure 3.

Combining the "CRADA" level of figure attained on an asphere in 1996 with the fact that commercial superpolishing currently attains finish levels better than required by EUVL suggests that a process can be developed for fabricating precise,* superpolished aspheres. However, in the next sections, we will present a rationale that strongly suggests that it is both feasible to fabricate aspheres that simultaneously meet the absolute accuracy and finish specifications in Table 1, but also that they will be available to meet the EUVL schedule requirements shown in Figure 1.

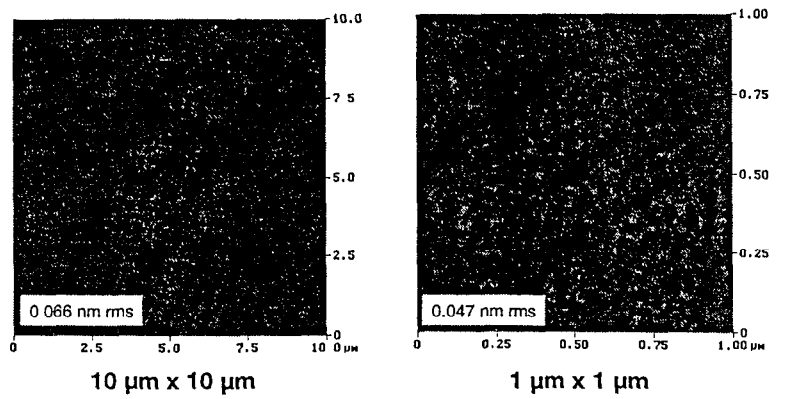

Figure 3. AFM micrographs of small superpolished BK7 lenses produced in production quantities by a commerial supplier.

Optical Finishing Development

The optical fabrication community has recently been addressing the fabrication of aspheric optical surfaces that meet stringent figure and finish specifications. One pertinent example is in the fabrication of lenses for UV and DUV lithography, where aspheres are employed to correct aberrations while minimizing the number of elements and the total optical path through glass.[16,17,18] Aspheric fabrication techniques are also being employed to compensate for refractive index variations in lenses and to improve the figure of spherical and flat surfaces that have errors remaining after traditional spherical and flat processing.

There is a growing effort in the optics community to improve aspheric fabrication technology in order to meet the future needs of EUVL.[14,19] Our program is assessing this rate of improvement by purchasing optical substrates from commercial supplier(s) using specifications that become increasingly stringent to keep pace with the required rate of development as shown in Figure 2. In this section, we review key measurements and observations that are drawn from our assessment. Note that this is an on-going process, and that the goal of this paper is to assess the feasibility of meeting EUVL specifications in a timely manner.

Our test and evaluation samples have been obtained from commercial source(s) and have all been fabricated using aspheric processing methods, although the surface contours are flat or spherical in order to simplify inspection. Some of the substrates have had simultaneous figure and finish specifications, while others have concentrated on improving finish while using aspheric methods. In all cases, the required specifications have been met.

The substrate materials include Zerodur,[20] Zerodur M,[20] and ULE.[21] Inspection of substrates of the different materials reveals subtle differences due to their differing microstructure, although we have not observed significant differences in their ability to meet figure and finish specifications. Further studies are underway to examine material selection issues.

The results for two of the developmental samples are shown in Figure 2. Sample C is a spherical substrate with specifications for figure, MSFR, and HSFR and provides an apples-to-apples comparison with the aspheric surfaces for the "Sandia 5x" measurements. The key observation is that even while maintaining figure

* The word *precise* is used here instead of *accurate* because the asphere fabricated in 1996 was compared to a reference that did not have an absolute calibration. However, the aspheres required to meet the EUVL specifications must be *accurately* fabricated with respect to the optical prescription. Thus there is a requirement for an instrument for measuring figure *accuracy*, which is addressed in a later section.

quality to about 0.6 nm rms, the values of MSFR and HSFR dropped to 0.51 nm rms and 0.20 nm rms, respectively. This level of figure improvement clearly meets the required rate of improvement indicated by the curves in the figure.

The goal of flat Sample E was to focus the aspheric processing development on improving surface finish, without a stringent specification on figure. Micrographs and roughness measurements for Sample E are shown in Figure 4 and Figure 5, which shows that rms roughness values are low, although artifacts of the material removal process, such as sleeking are visible. The MSFR value of 0.30 nm rms and HSFR value of 0.14 nm rms are plotted on the timeline in Figure 2. Both of these values are closely approaching the final EUVL specifications.

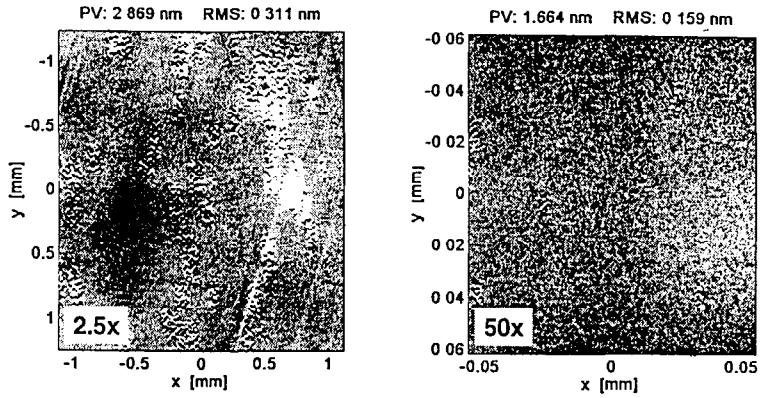

Figure 4. Phase-shifting interference microscopy indicates improved levels of finish on Zerodur M Sample E prepared using aspheric methods.

A measure of the improvement in the functionality represented by these reductions in surface roughness is indicated in Figure 1, where reflectivities for two developmental flat samples is indicated. The reflectivity for an earlier sample, BZM, was measured at the Advanced Light Source at LBNL as 59%. The 64% reflectivity for Sample E was estimated by calculating the angular distribution of scattered light from the measured roughness.[22] The estimated system throughput for a system with mirrors of the same roughness as Sample E is 17%, which is converging to the throughput goal of 20% .

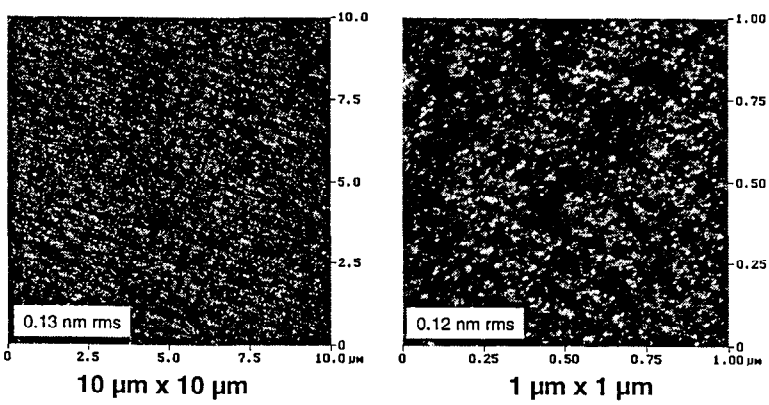

Figure 5. Atomic force micrographs indicate that aspheric processing on Zerodur M Sample E nearly meets the EUVL specification for HSFR.

Intermediate Milestone

The first substrate (M3) of a 4-mirror system fabricated to the "intermediate specifications" shown in Figure 2 was completed by a commercial supplier as this manuscript was being prepared. Initial figure and finish measurements are shown in Figure 6, with measured values of 0.44 nm rms for figure and 0.31 nm rms for finish as measured using a phase-shifting interferometric microscope. Both of these values are significantly better than the "intermediate specifications", although a true comparison with specifications will require an integration of the power spectral density in accordance with the definitions in Table 1. A preliminary estimate suggests that the value for MSFR will be around 0.25 nm rms, which is very close to the final EUVL specification of 0.20 nm rms.

The contour of M3 is spherical, although the vendor indicates that aspherical methods were used to attain the low figure errors. The map of figure errors shown in Figure 6 shows a shallow rippled pattern with spatial wavelengths of about 1-5 mm, combined with longer spatial wavelength zonal errors.[23] Because of this success in

employing aspherical methds, we anticipate that aspherical surfaces that do not significantly deviate from a spherical shape are also fabricable to the same high degree of accuracy as M3.

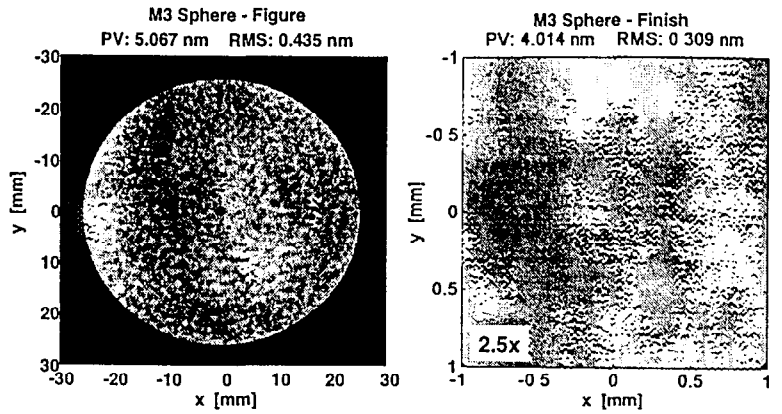

Figure 6. M3 is the first of the Zerodur M substrates to be completed to the "intermediate specifications" shown in Figure 2; although the contour is spherical, aspherical processing methods were used to attain excellent figure and finish.

Calculation of Surface Errors

As noted in the definition of the specifications given in Table 1, the relevant parameter is the rms power obtained by integrating the 2-D power spectral density (PSD) over an appropriate band of spatial frequencies. The use of 1-D PSDs is well-described in the literature, particularly in relating light scattering to surface statistics.[24,25] However, the calculation of statistics from the 2-D PSD is relatively uncommon, although there is a trend for its increasing application.[26,27] In this section we will graphically describe the procedure for calculating the 2-D bandlimited rms power.

The 2-D PSD is calculated as

$$S(f_x, f_y) = \frac{L_x L_y}{M^2 N^2} \left| \sum_{m=0}^{M-1} \sum_{n=0}^{N-1} z(x_m, y_n) e^{-2\pi i m \Delta x f_x} e^{-2\pi i n \Delta y f_y} \right|^2 \quad (1)$$

where z(x,y) is the distribution of surface errors over the x,y plane
L_x, L_y are scan lengths in the x and y directions
f_x, f_y are spatial frequencies in the x and y directions
M, N are the number of equi-spaced samples in the x and y directions
Δx, Δy are the sample spacings for x and y

Essentially, Eq. 1 states that the 2-D PSD is the squared magnitude of the 2-D Fourier transform of the surface errors. Reference [24] presents a good introduction of several subtleties that can confuse the calculation of PSDs, such as windowing and the use of averaging to drive down noise and uncertainty.

Figure 7 illustrates the 2-D PSD of an AFM measurement, shown in the upper left hand corner, which was calculated by applying Eq. 1 (without window).[28] The out-of-plane height of the image is the 2-D PSD in units of nm^4, while the x,y plane denotes spatial frequency [cycles per micron] in the x and y directions. The frequency axes extend from the negative Nyquist frequency to the positive Nyquist frequency, where the center represents lower frequencies. This chart illustrates that power is calculated for both positive and negative frequencies, and care must be exercised to account for both sides of the frequency axes. The contribution to the PSD from waviness oriented in a particular direction is found by observing the *radial PSD* along the given coordinate direction. A particular radial PSD can be plotted on a 1-D plot, but with units of the 2-D PSD. We delimit our analysis within the 2-D PSD domain to spatial frequencies that fall within a circle with a radius of the

Nyquist frequency (or an ellipse if the Nyquist frequencies are different in the x and y directions). As shown in the figure, there is power in the corner regions of the 2-D PSD that we omit from the analysis.

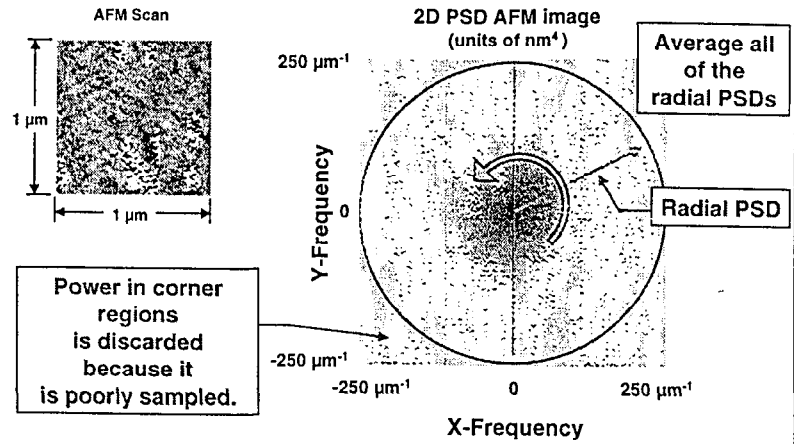

Figure 7. The power of the surface roughness is calculated by considering the average radial PSD determined from a circular region within the 2-D PSD.

It is important to note that the PSD given in Figure 7 only incorporates power that is within the bandwidth of the instrument or has not been otherwise removed by any filtering or detrending. The rms power (commonly referred to as the "rms surface roughness") for a particular frequency bandwidth (e.g. from 1 cycle/µm to 100 cycles/µm) can be found by integrating the volume under an annular region in the 2-D PSD plot, where the radial limits of the annulus extend between the two frequency limits.

A numerically equivalent approach which offers additional insight into the PSD is offered by first calculating the average radial PSD. As illustrated in the 2-D plot, we consider the collection of all radial PSDs, and then calculate the average. This results in a PSD that can be viewed on a 1-D PSD plot, shown in Figure 8, although the units are still those for the 2-D PSD, i.e. (length)^4. This radial PSD can be examined for peaks corresponding to particular waviness characteristics such as might be indicative of "orange peel". Because the power in this plot is averaged over 2π, the average radial PSD will have reduced sensitivity for indicating waviness in a specific direction, such as for a grating. Although not shown here, another useful technique is to examine the variation of the 2-D PSD with coordinate direction in order to obtain additional information regarding the lay of the surface.[26]

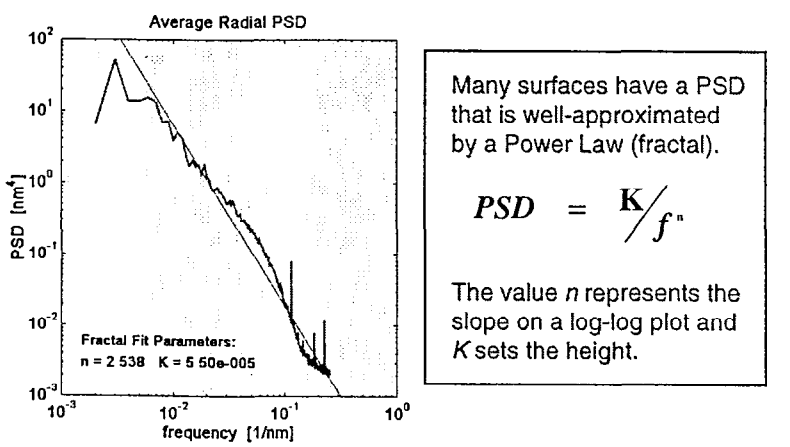

Figure 8. The average radial 2-D PSD can be plotted on a 1-D PSD plot, but with units of (length)^4; in this format, 1-D analysis methods, such as determining fractal parameters, can be employed.

Many well-polished surfaces have a PSD (1-D and average radial) that is approximately linear on a log-log plot, which indicates a fractal surface finish.[29] For example, in Figure 8, a best fit line is drawn for comparison with the average radial PSD. The equation for the straight line, commonly called a *fractal fit*, is shown in the figure and has parameters K and n which set the height and slope, respectively. Generally, for higher slopes, the lower frequencies have a greater relative importance. Note that the exact definition of the parameter K will depend on the mathematical formalism employed and if any constants are factored out of the above definition.

To find the power corresponding to a particular frequency band, the average radial PSD can be integrated by revolving it about the origin to form the average 2-D PSD, and then integrating between annular frequency limits, as mentioned before. This procedure is analogous to calculating the volume under a surface of revolution using the Theorems of Pappus.[30] If a fractal fit is a good approximation for the average PSD, the integral for calculating the rms height is given in Figure 9; also given is the integral for calculating the rms slope from the using the fractal fit. It is important to note that these specific formulations are only appropriate when the fractal fit is for the average radial PSD, not for a fit to the 1-D PSD.

$$\sigma^2 = \int_{f_1}^{f_2} \frac{2\pi K f}{f^n} df = \left[\frac{2\pi K f^{2-n}}{2-n} \right]_{f_1}^{f_2}$$

$$\mu^2 = \int_{f_1}^{f_2} \frac{2\pi K f}{f^n} (2\pi f)^2 df = \left[\frac{8\pi^3 K f^{4-n}}{4-n} \right]_{f_1}^{f_2}$$

σ = rms height μ = rms slope

Figure 9. Integrals for calculating the rms height and the rms slope using fractal fit parameters for the average radial PSD of surface height errors.

Metrology for EUVL Optics

The bandwidths of the three specification categories given in Table 1, figure, MSFR, and HSFR, correspond approximately to the bandwidths measured by three types of instruments: full-aperture phase-shifting interferometry, phase-shifting interferometric microscopy, and atomic-force microscopy (AFM), respectively. Thus, power spectral densities can be assembled that cover an extremely wide spatial frequency band, i.e. CA^{-1} to 0.1 nm^{-1}. It is outside of the scope of this paper to provide a comprehensive discussion of these types of measurements.

We are employing a commercially-available AFM with sufficient vertical and horizontal resolution to characterize sub-0.1 nm rms surfaces with evidence of the material microstructure and the material removal process. The noise level of the measurements is typically 0.03 nm rms, and we typically use a new stylus for each measurement of every smooth surface. Although images of the surface are easily analyzed and interpreted as surface height data, we are currently examining the errors associated with the measurement and the ability to employ the AFM data as a certifiable measure of the surface. Fortunately, we see an excellent correlation between PSDs measured using the AFM and PSDs that are inferred from angle-resolved scattering measurements.[22]

Our phase-shifting interferometric microscope is also a commercial unit with multiple objectives for covering the spatial frequency band extending from 1 mm^{-1} to 1 μm^{-1}. Our surfaces typically have features below the instrument vendor's stated resolution, yet we observe a clear relationship between roughness and scattering data. We have noticed some anomalies in the data, however, such as a tendency for interferometer fringes to print through to phase maps when measuring curved surface (sometimes referred to as *residual fringes*). Fortunately the levels of these "errors" have not prevented us from making useful characterizations of our current surfaces, although we are in the process of identifying the source(s) for the anomalies.

We have designed and built a phase-shifting diffraction interferometer (PSDI) for measuring the figure accuracy of EUVL mirror substrates.[31] A visible light interferometer is attractive for measuring figure for several reasons: the unit of measure is the testing wavelength λ_v, which is stable and traceable and can be further subdivided to give increased resolution; the surface of the optic under test can be spatially sampled at many points ($>10^5$) simultaneously; the data acquisition time is less than one second; and it can easily be set up and operated

in optical shops. For the characterization of most optics, where $\lambda_w/20$ to $\lambda_w/50$ rms accuracy is sufficient, commercial interferometers are adequate. However for EUV optics this is not the case. For typical testing wavelengths, $\lambda_w/50$ corresponds to a factor of 40 to 50 larger than the accuracy required for EUV mirrors.

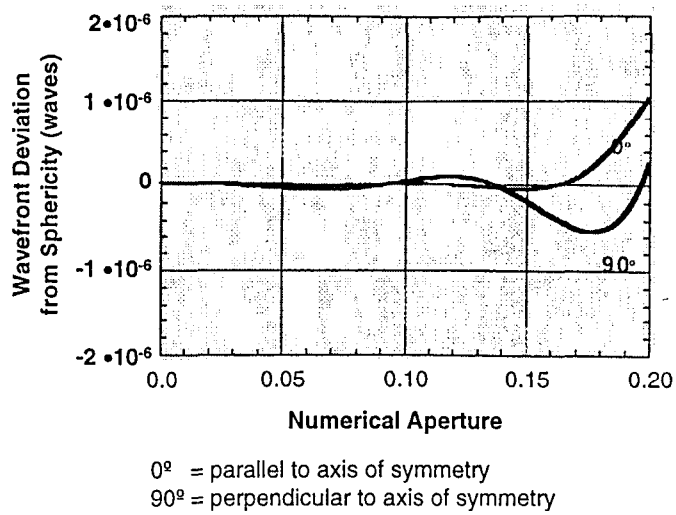

Figure 10. Calculated deviation from sphericity for reference waves generated by a diffracting aperture.

The accuracy (agreement between a measured value and the true value) of surface figure interferometers is limited by several factors. Since interferometry is a comparative technique, the quality of the reference directly affects the accuracy of the measurement. This is the primary source of error in an interferometer. This error has been minimized by using phase shifting diffraction interferometry, where the fundamental process of diffraction is used to generate two arbitrarily perfect spherical wavefronts - one serves as the measurement wavefront and is incident on the mirror surface under test and the other serves as the reference wavefront. Figure 10 shows that the calculated deviation from sphericity for reference waves generated with a diffracting aperture are negligible. Since they are generated independently, their relative amplitude and phase can be controlled, providing contrast adjustment and phase shifting capability. This concept has been implemented in several different ways using lithographically generated apertures or single mode optical fibers.

The PSDI, configured to measure a concave mirror, is shown in Figure 11. Two temporally incoherent beams are launched into the same optical fiber. One beam is phase shifted by reflection from a retroreflector mounted on a PZT. The other beam is time delayed with an adjustable beam path to equal to the round-trip distance between the fiber face and the mirror under test. Interference on the CCD camera takes place between the phase-shifted wavefront that is reflected from the optic under test and the delayed wavefront directly from the fiber. The mirror surface is imaged onto the CCD camera and data acquisition and analysis are similar to other phase shifting interferometers.

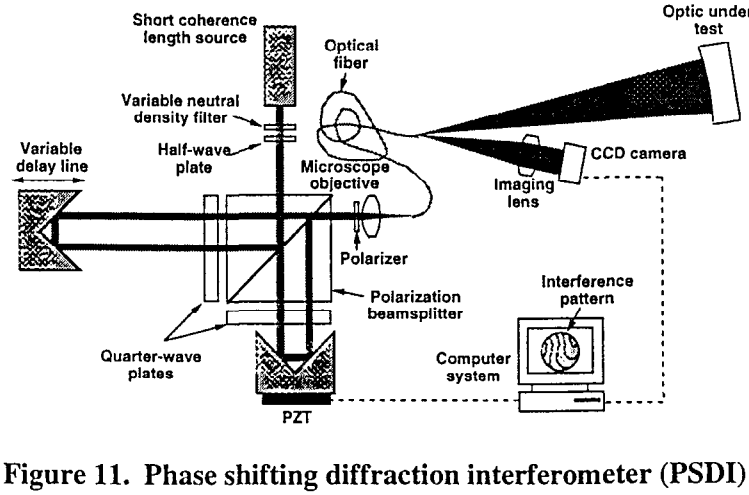

Figure 11. Phase shifting diffraction interferometer (PSDI) set-up for measuring a concave surface (the PSDI is patented).

An important requirement of the PSDI is the ability to measure aspheric surfaces.[32] The PSDI relies on spherical reference waves, and in order to achieve the required accuracy, we cannot employ null-type surfaces. Therefore, we have developed a method where we employ the fringe pattern generated by using the spherical reference, but avoid the regions of high fringe density that lead to increased errors. This is accomplished

by stitching together multiple phase maps, where each highlights a different region of the clear aperture with a near-null fringe density. This is accomplished by sequentially translating the surface under test to produce a null fringe pattern at a given location, making a measurement, and then translating the surface to move the null region to another location, and so on until all locations within the clear aperture have been measured at least once with a near-null fringe density. We then employ a newly developed algorithm for stitching together all of the phase maps, such that all of the near-null regions are retained, and all of the regions of high fringe density are omitted. Typical EUVL aspheres require only two measurements, i.e. only one stitch. Thus far, we have certified a clear aperture for an aspheric ring-field field using only two stitched regions yielding a final surface accuracy of about 0.9 nm rms. Our calculations indicate that errors associated with this stitching procedure can be driven well below the level required for measuring the aspheres used in the current 4-mirror design.

Conclusions

The Extreme Ultraviolet Lithography Program requires mirror substrates with stringent specifications for figure and finish that are currently beyond the state-of-the-art in fabrication technology. Nevertheless, there is significant progress and momentum in developing new finishing processes for lithographic aspheres, that it is clearly feasible to meet the EUVL specifications and schedule requirements. The optics industry is currently attaining figure and finish levels near those required for EUVL aspheres: 0.30 nm rms for figure, 0.3 nm rms for mid-spatial frequency errors, and 0.13 nm rms for high-spatial frequency errors. The rate at which finishing performance is improving will enable a projection optics system to be assembled for successfully meeting current EUVL program requirements.

Acknowledgments

The authors owe special appreciation to Sherry Baker (LLNL) for making many of the AFM measurements, John Bjorkholm (Intel) for discussions on flare and scattering, Jay Daniel (SVG-Tinsley) for figure and finish measurements, and Eric Gullikson (LBNL), Eberhard Spiller, and Dan Stearns (OS Associates) for discussions on power spectral density, scattering, and multilayers. This work was performed under the auspices of the U.S. Department of Energy by the Lawrence Livermore National Laboratory under Contract No. W-7405-ENG-48. Funding was provided by the Extreme Ultraviolet Limited Liability Corporation under a Cooperative Research and Development Agreement.

Notes and References

[1] **Extreme Ultraviolet Lithography**, *Trends in Optics and Photonics* (TOPS), vol. IV, G. D. Kubiak and D. R. Kania eds., Optical Society of America (1996).

[2] Hawryluk, A. M., Ceglio, N. M., Markle, D. A., "EUV Lithography", **Microlithography World**, vol. 6, no. 3, Summer 1997, p. 17.

[3] Goldsmith, J. E. M., et. al., "Recent advances in the Sandia 5x microstepper", in **Emerging Lithographic Technologies II**, Proc. SPIE, vol. 3331, 1998 (paper 3331-02 to be published; this proceedings).

[4] Sweeney, D. W., et. al., "EUV optical design for a 0.1 μm imaging system", in **Emerging Lithographic Technologies II**, Proc. SPIE, vol. 3331, 1998 (paper 3331-01 to be published; this proceedings).

[5] As a further comparison between DUV and EUV systems, consider a hypothetical 193 nm imaging system with 30 elements (60 surfaces) with a refractive index of 1.5, separated by vacuum. The composite WFE can be estimated as the RSS of the average WFE contribution from each of the 60 surfaces:

$$0.07(193) = \sqrt{60\left(\overline{wfe}\right)^2} \quad \text{which yields } \overline{wfe} = 1.74 \text{ nm}$$

For this transmissive system, the figure accuracy for each surface is approximated as $\overline{wfe}/(n_2 - n_1) \approx 2\,\overline{wfe} = 3.5$ nm rms. Thus the ratio of acceptable surface errors for DUV and EUV is 3.5 nm/0.25 nm ≈ 15 but will depend on the exact number of surfaces used in the system. Clearly this calculation is an approximation, where the allowable errors on any particular element are obtained from a detailed element-by-element error.

[6] Kirk, J. P., "Scattered light in photolithographic lenses", in **Optical/Laser Microlithography VII**, Proc. SPIE vol. 2197, 1994, pp. 566-572.

[7] Park, J., et. al., "Measuring flare and its effect on process latitude", in **Optical Microlithography X**, Proc. SPIE vol. 3051, pp. 708-723, 1997.
[8] Progler, C., du, H., Wells, G., "Potential causes of across-field CD variation", in **Optical Microlithography X**, Proc. SPIE vol. 3051, pp. 660-671, 1997.
[9] Montcalm, C., et. al., "Multilayer reflective coatings for extreme-ultraviolet lithography", in **Emerging Lithographic Technologies II**, Proc. SPIE, vol. 3331, 1998 (paper 3331-05 to be published; this proceedings).
[10] Windt, D. L., Waskiewicz, W. K., and Griffith, J. E., "Surface finish requirements for soft x-ray mirrors", **Applied Optics**, vol. 33, no. 10, pp. 2025-2031 (1 April 1994).
[11] The reflectivity numbers mentioned in the figure are normalized to a common detector size by considering scattering outside of a 0.1 μm image feature, and thus include the effects of scatter due to both MSFR and HSFR.
[12] Tichenor, D. A., et. al., "Progress in the development of EUV imaging systems", in **Extreme Ultraviolet Lithography**, *Trends in Optics and Photonics* (TOPS), vol. IV, G. D. Kubiak and D. R. Kania eds., Optical Society of America, pp. 2-8 (1996).
[13] Gaines, D. P., et. al., "Surface characterization of optics for EUV lithography", in **Extreme Ultraviolet Lithography**, *Trends in Optics and Photonics* (TOPS), vol. IV, G. D. Kubiak and D. R. Kania eds., Optical Society of America, pp. 103-106 (1996).
[14] Kestner, R., "Precision asphere fabrication and metrology to tolerances <1 nm rms", paper presented at the OSA Optical Fabrication and Testing Topical Meeting, Boston, May 1-3, 1996; note that this measured value represents the difference with respect to the vendor's interferometric reference, not a definitive statement of accuracy.
[15] *Superpolishing* is a jargonal term that often has different meanings within different companies; in this paper, and commonly in the EUV community, *superpolishing* refers to surfaces with MSFR and HSFR at or below 0.1 nm rms, which coincides with specifications encountered for laser gyro mirrors; for example, see Brown, N. J., "Preparation of ultrasmooth surfaces", **Ann. Rev. Mater. Sci.**, vol. 16, 1986, pp. 371-388.
[16] Bajuk, D., "Computer controlled fabrication of microlithographic aspheres", paper presented at the US-Japan Workshop on EUV Lithography, October 27-29, 1993, Mt. Fuji, Japan.
[17] Carbone, F. A. and Markle, D., "Combining ion figuring and SPSI testing to produce a high quality, aspheric, 18" diameter, f/2 mirror", in **Optical Manufacturing and Testing**, Proc. SPIE, vol. 2536, pp. 89-98 (1995).
[18] "SVG Litho, NASA enter optical collaboration", **Wafer News**, vol. 4.9, March 10, 1997.
[19] Kania, D. R., et. al., "Precision optical aspheres for extreme ultraviolet lithography", **J. Vac. Sci. & Tech.**, vol. 14, no. 6, Nov./Dec. 1996, pp. 3706-3708.
[20] *Zerodur* and *Zerodur M* are manufactured by Schott Glass Technologies, Inc.
[21] *ULE* is manufactured by Corning, Inc.
[22] Excellent agreement has been demonstrated in relating the angular distribution of scattered light to the power spectral density of surface roughness; see Gullikson, E. M., "Nonspecular scattering for normal-incidence EUV optics", in **Emerging Lithographic Technologies II**, Proc. SPIE, vol. 3331, 1998 (paper 3331-08 to be published; this proceedings).
[23] Several computer controlled material removal methods using 'small tools' are described in **Selected Papers on Computer-Controlled Optical Surfacing**, R. A. Jones, editor, SPIE Milestone Series, vol. MS40, 1991.
[24] Elson, J. M. and Bennett, J. M., "Calculation of the power spectral density from surface profile data", **Applied Optics**, vol. 34, no. 1, pp. 201-208 (1 Jan 1995).
[25] Church, E. L. and Takacs, P. Z., "Specification of glancing- and normal-incidence x-ray mirrors", **Optical Engineering**, vol. 34, no. 2, pp. 353-360 (Feb. 1995).
[26] Stout, K. J., et. al., **The Development of Methods for the Characterization of Roughness in Three Dimensions**, published on behalf of the Commission of the European Communities by the Univ. of Birmingham, Great Britain, pub. No EUR 15178 EN, pp. 187-193 (1993) [ISBN 0 7044 1313 2].
[27] Lawson, J. K., et. al., "Specification of optical components using the power spectral density function", in **Optical Manufacturing and Testing**, Proc. SPIE, vol. 2536, 1995, pp. 38-50.
[28] The software used is *PSDMaker* by D. G. Stearns, OS Associates, 1174 Castro St., Suite 250, Mountain View, CA 94040.
[29] Church, E. L., "Fractal surface finish", **Applied Optics**, vol. 27, no. 8, pp. 1518-1526 (15 Apr 1988).
[30] The Theorems of Pappus are given in most textbooks on analytic geometry, e.g. Protter, M. H. and Morrey, Jr., C. B., **College Calculus with Analytic Geometry**, Addison Wesley, Menlo Park, CA (1970).
[31] Sommargren, G. E., "Phase shifting diffraction interferometry for measuring extreme ultraviolet optics", in **Extreme Ultraviolet Lithography**, *Trends in Optics and Photonics* (TOPS), vol. IV, G. D. Kubiak and D. R. Kania eds., Optical Society of America, pp. 108-112 (1996).
[32] Campbell, G., Sommargren, G. E., Phillion, D. W., "Measurement of aspheres using phase shifting diffraction interferometry", paper presented at the OSA Annual Meeting and Exhibit, October 20-24, 1996, Rochester, NY.